Enhanced near-field radiation in both TE and TM waves through excitation of Mie resonance

Yizhi Hu,[1] Hongen Li,[1] Yong Zhang,[2] Yonggang Zhu,[1] and Yue Yang[1,*]

[1]*School of Mechanical Engineering and Automation, Harbin Institute of Technology, Shenzhen 518055, People's Republic of China*

[2]*School of Energy Science and Engineering, Harbin Institute of Technology, Harbin 150001, People's Republic of China*

(Received 23 March 2020; revised 27 August 2020; accepted 11 September 2020; published 28 September 2020)

Near-field radiative heat transfer between two bodies can exceed the far-field blackbody limitation predicted by Planck's law due to the evanescent waves tunneling or coupling of additional surface modes, which typically can occur only in TM modes for nonmagnetic materials. The Mie resonance may have the potential to enhance near-field radiation in both TM and TE modes according to the calculated results from effective medium theory. However, there is no exact solution to verify this to date. In this paper, we will give a rigorous numerical investigation of the role of Mie resonance in near-field radiative heat transfer. The framework of fluctuational electrodynamics that combines scattering matrix theory with the rigorous coupled wave analysis method is used to exactly compute the near-field radiative flux between Mie resonant dielectric cubic arrays. It shows that due to the excitation of Mie resonance, causing ε/μ near-pole effects, the radiative heat flux could be spectrally enhanced in TM/TE modes. The discrepancy between the effective medium theory and the exact method is also elucidated in detail. The findings will provide a way to control near-field thermal spectrum via all-dielectric metamaterials for emerging thermal technologies.

DOI: 10.1103/PhysRevB.102.125434

I. INTRODUCTION

When the gap spacing between two bodies is comparable to or smaller than the thermal wavelength concerned, the evanescent waves induced by thermal fluctuations can tunnel through the gap spacing, and the radiative heat flux can be significantly enhanced, exceeding the blackbody limitation predicted by Planck's law [1,2]. In particular, if surface modes are excited, like surface plasmon polaritons in metals or doped silicon [3,4] and surface phonon polaritons in silicon carbide [5,6], the radiative heat flux can be further increased, and the corresponding spectral heat exchange shows a monochromatic or quasimonochromatic effect. In comparison with the case of bulk materials, the near-field thermal transport between different extended structures [7] can be improved again due to resonant coupling of hyperbolic polaritons [8,9], magnetic polaritons [10,11], or spoof surface plasmon polaritons [12,13]. However, few modes are supported in TE waves for these nonmagnetic systems. Electromagnetic metamaterials [14], which are artificially engineered materials with unusual electric and magnetic properties, can develop electric and magnetic surface modes in TE and TM polarizations simultaneously as a result of the plasmonic or resonant behavior of the constitutive elements. Thus, a plethora of studies focused on hypothetical metallic metamaterials, which have been proved to be able to mediate near-field radiative heat transfer [15–20]. Near-field thermal radiation could find many attractive applications, such as cooling of electronics [21], thermal management [22–25], and thermophotovoltaic systems [26].

All-dielectric metamaterials based on Mie resonance [27] can generate an electric and magnetic response for TE and TM polarization, respectively. According to Mie theory [28], waveguide modes will be exhibited when plane electromagnetic waves are incident on a microstructured trap made of dielectric material with high permittivity, bringing out the excitation of Mie resonances. The first-order and second-order Mie resonances can be equivalent to the magnetic and electric dipoles in TE and TM modes, respectively [29]. These magnetic and electric dipole resonances acting as artificial elements cause Lorentzian-type dispersions, which form macroscopic negative permeability and permittivity in some specific spectral bands [30]. Previous studies have shown that surface polaritons (SPs) in both TE and TM modes incurred by negative permeability and permittivity can be used for regulating near-field radiative heat flux [31–33]. Several theoretical studies [34,35] have provided a comprehensive procedure for investigating the properties, effects, and local density of electromagnetic states originating from Mie resonant metamaterials on near-field radiation and regarded the host material containing spherical dielectric inclusions to be an effective isotropic medium with negative permittivity and permeability via the macroscopic approximation of the Clausius-Mossotti model. Based on this kind of effective medium theory (EMT), a Mie resonant thermal emitter for near-field thermophotovoltaic systems [36] was devised, and the sensitivity of emitter design parameters [37] was quantitatively analyzed. However, to the best of our knowledge, there is no exact solution to check and verify the performance of Mie resonance on near-field radiation to date, and only EMT is not sufficient considering the validity of EMT for such a configuration has not been confirmed. This paper describes an exact numerical investigation of Mie resonance in the

*Corresponding author: yangyue2017@hit.edu.cn

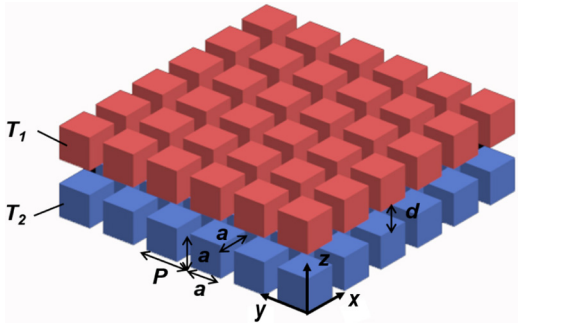

FIG. 1. Schematic of radiative transfer between two symmetric, perfectly aligned 2D periodic arrays of cubes with parameters of period P and side length a held at temperatures T_1 and T_2. The vacuum gap distance is denoted as d.

near-field radiative transfer between two all-dielectric metasurfaces separated by a vacuum gap. We will also reveal the discrepancy between the EMT and exact solution for predicting the near-field radiative heat flux.

II. NUMERICAL METHOD

The system that we study in this paper is depicted in Fig. 1. It consists of two identical, perfectly aligned metasurfaces formed by two-dimensional (2D) periodic arrays of cubes. The temperatures of the emitter and receiver are set as T_1 and T_2 and kept unchanged. The geometrical parameters of the metasurface structure are the lattice constant P, the side length of cubes a, and the gap size d. A similar geometric structure utilizing doped silicon was adopted to understand the excitation of hyperbolic modes [38]. Here we fix the lattice constant P at 3.4 μm and investigate the effect of Mie resonance on radiative heat flux through changing the side length of cubes a. The side length a varies from 1.5 to 1.7 μm in an increment of 0.1 μm. In order to excite Mie resonance and obtain a double-negative property, cubic resonators with large relative permittivity values ε' and low dielectric loss are required [30]. Hence, for this study, tellurium is selected as the resonator material, which yields a complex dielectric constant with low loss angle $\varepsilon = 25 + 0.4i$ (i.e., loss angle $\tan\delta = 0.016$) at infrared frequencies [39].

To obtain the exact near-field radiative heat flux of the periodic cubic resonator system, we combine the dyadic Green's function method with rigorous coupled wave analysis (RCWA) [40] to compute it. According to the fluctuational electrodynamics theory, thermal radiation originates from random current sources inside the emitter, which are related by the fluctuation-dissipation theorem,

$$\langle \mathbf{J}(\mathbf{r}, z, \omega)\mathbf{J}^*(\mathbf{r}', z', \omega')\rangle = \frac{4\varepsilon_0\omega}{\pi}\Theta(\omega, T)\delta(z - z')\delta(\omega - \omega')\Gamma, \quad (1)$$

where the tensor Γ with indexes is defined as $\Gamma_{\alpha\beta} \equiv \varepsilon''_{\alpha\beta}\delta(\mathbf{r} - \mathbf{r}')$, $\mathbf{R} = (\mathbf{r}, z)$ or $\mathbf{R}' = (\mathbf{r}', z')$ is a field point in the x-y plane, $\delta(\cdot)$ is the Dirac function indicating the locality of real and frequency spaces, and $\varepsilon''_{\alpha\beta}$ is the imaginary part of the dielectric tensor, with α and β denoting components in three-dimensional real space. $\Theta(\omega, T) = \hbar\omega/[\exp(\hbar\omega/k_BT) - 1]$ is the mean energy of a Planck oscillator in thermal equilibrium at a frequency ω and temperature T. The radiative heat flux $q(\omega, T)$ can be acquired by calculating the ensemble-averaged Poynting vector along the z direction. The averaged spectral Poynting flux density along the z direction emitted from the source point z' in one unit cell can be written as

$$\langle S_z\rangle = \frac{\Theta(\omega, T)}{A}\Phi(\omega). \quad (2)$$

$\Phi(\omega)$ is called the transmission factor, which can be expressed as

$$\Phi(\omega) = \frac{2\omega\varepsilon_0}{\pi}\int \mathrm{Re}\{\mathrm{Tr}[\Pi^{\mathrm{T}}\mathbf{G}_e\Gamma\mathbf{G}_h^{\dagger}]\}dz', \quad (3)$$

where ε_0 is the vacuum dielectric constant, A is the area of the unit cell, Π is the Levi-Civita tensor, and $\mathbf{G}_e$ and $\mathbf{G}_h$ are the dyadic Green's operators relating the electromagnetic field $\mathbf{E}$ and $\mathbf{H}$ observed at $\mathbf{R}$ to the source point at $\mathbf{R}'$, i.e., $\mathbf{E} = \mathbf{G}_e\mathbf{J}$ and $\mathbf{H} = \mathbf{G}_h\mathbf{J}$. For our system, the near-field transmission factor $\Phi(\omega)$ is calculated by integrating the transmission coefficient $\xi(\omega, \mathbf{k}_\parallel)$ over all possible directions of the in-plane wave vector $\mathbf{k}_\parallel$. The transmission coefficient ξ that characterizes the probability of a thermally excited photon transferring from one metasurface to the other can be obtained by the RCWA method, which is described in Appendix A.

III. RESULTS AND DISCUSSION

Let us start the discussion of the results by illustrating the main findings of our work. The spectral radiative heat flux $q(\omega, T_1, T_2)$ can be obtained by the spectral transmission factor $\Phi(\omega)$ multiplied by $\Theta(\omega, T_1) - \Theta(\omega, T_2)$. We plot three radiative heat flux spectra between two cubic dielectric metasurfaces at a vacuum gap distance of $d = 1$ μm with dissimilar side lengths a from 1.5 to 1.7 μm in Fig. 2. The emitter temperature $T_1 = 600$ K and receiver temperature $T_2 = 300$ K are fixed throughout the paper unless otherwise noted. For the

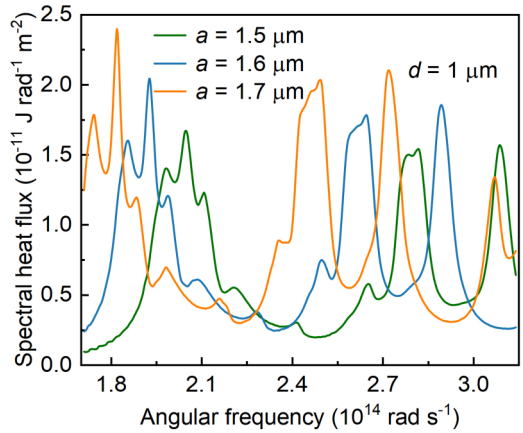

FIG. 2. Spectral heat fluxes between the two cubic dielectric resonators at a vacuum gap of $d = 1$ μm with different side lengths a.

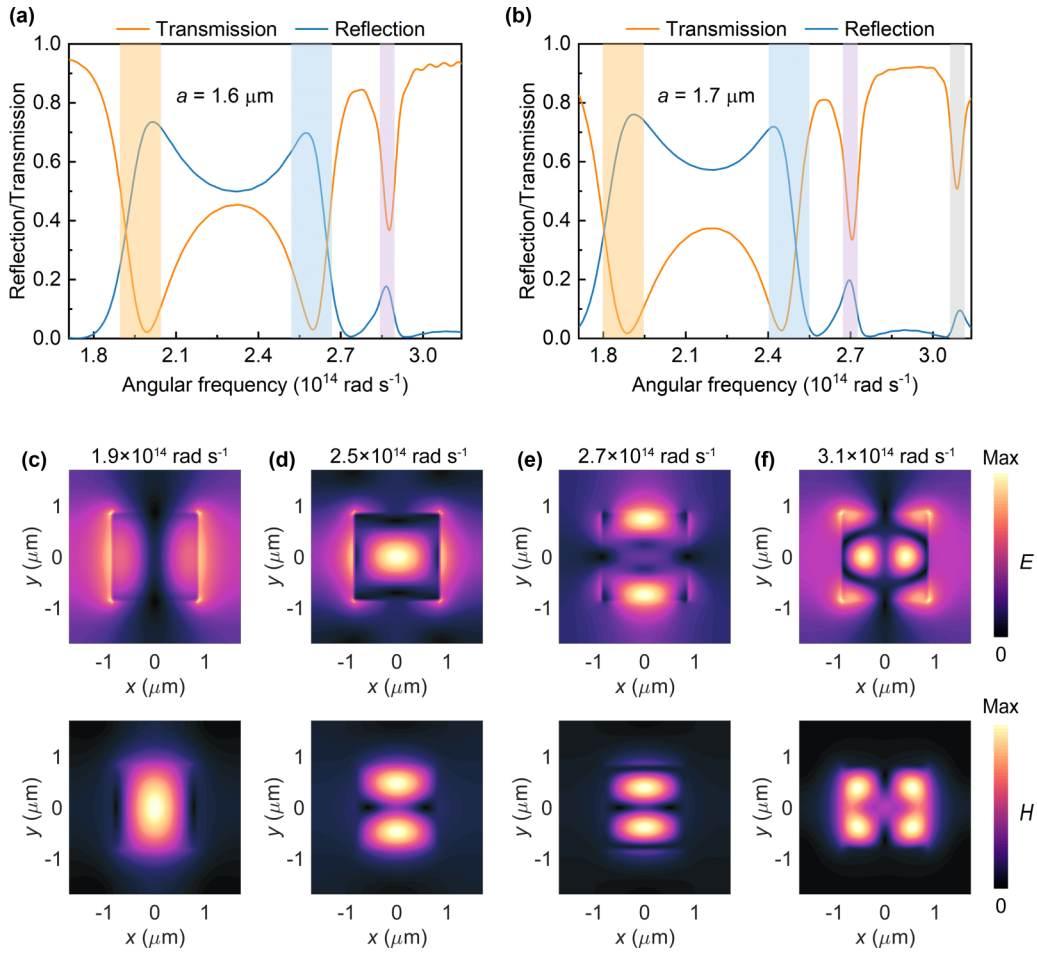

FIG. 3. Reflection and transmission of the cubic dielectric resonator array with side length (a) $a = 1.6$ μm and (b) $a = 1.7$ μm. The orange, blue, purple, and gray areas mark the Mie resonant region. The corresponding electromagnetic field intensity distributions E_{xy} and H_{xy} are shown for (c) the magnetic dipole, (d) the electric dipole, and (e) and (f) higher-order resonant modes.

parallel metasurfaces, the spectral heat flux curves exhibit a series of peaks whose frequency locations shift as a changes. When a increases, the peaks shift towards lower frequencies, and the relative locations between them remain unchanged. Moreover, the amplitudes of those increase slightly as a increases.

To explore the physical mechanisms responsible for these spectral heat flux peaks, the reflection and transmission spectra of a single metasurface, i.e., the emitter or receiver shown in Fig. 1, calculated based on the finite-difference time-domain (FDTD) method in the far-field regime are presented in Figs. 3(a) and 3(b). In both plots, the spectral bands where Mie resonant modes may exist are shaded different colors. The geometrical and material parameters applied here are the same as those used in near-field investigation. As one can see, there is a host of peaks and dips in the far-field reflection/transmission spectra of the metasurface as well. In Fig. 3(b), as $a = 1.7$ μm, four separate peaks and dips are observed at frequencies around $\omega = 1.9$, 2.5, 2.7, and 3.1×10^{14} rad/s, corresponding to different Mie resonant modes. In order to confirm that Mie resonance is excited in such a metasurface, Figs. 3(c)–3(f) depict on-resonance electromagnetic field intensity distributions E_{xy} and H_{xy} at each peak frequency to reveal the Mie scattering characteristics [41]. When the incident plane waves with frequencies of 1.9 and 2.5×10^{14} rad/s hit the high-index cubic array, it is evident that magnetic and electric dipole resonances are excited in Figs. 3(c) and 3(d), respectively, making the cube behave like a magnetic dipole (first-order Mie resonance) and an electric dipole (second-order Mie resonances). It should be noted that the magnetic resonance possesses unique circular displacement currents, which are capable of coupling with evanescent waves and enhancing the near-field radiative heat flux. As for electromagnetic waves at 2.7 and 3.1×10^{14} rad/s, pronounced higher-order Mie resonance will appear, resembling in such a manner the magnetic/electric quadrupole and octupole configurations in Figs. 3(e) and 3(f).

To understand the role of Mie resonance in near-field radiative flux, the Mie effective medium theory (MEMT) approximation is considered, which describes the metasurface as a monolithic medium with macroscopic electric and magnetic responses via an effective electric permittivity ε_{eff} and an effective magnetic permeability μ_{eff}. Based on the mean-field approximation, the S-parameter retrieval method [42] is proposed to characterize ε_{eff} and μ_{eff} of the metasurface. The

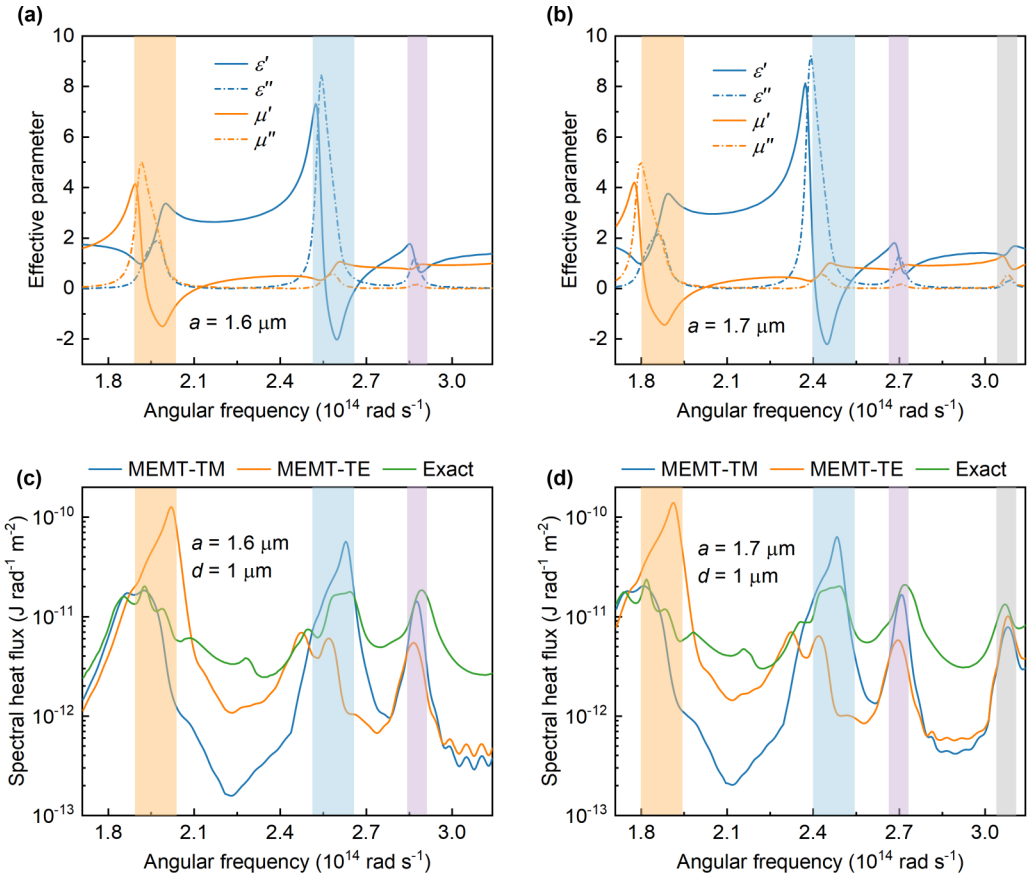

FIG. 4. (a) and (b) Effective parameter of the cubic dielectric resonator array, calculated for different side lengths a. Solid and dot-dashed lines indicate real and imaginary parts, respectively. Spectral heat fluxes between the Mie resonant emitter and receiver at different side lengths of (c) $a = 1.6$ μm and (d) $a = 1.7$ μm obtained from the exact method (denoted as "exact") in comparison with those in TE modes and TM modes from Mie effective medium theory (denoted as "MEMT-TE" and "MEMT-TM," respectively).

equations used by the S-parameter method are as follows:

$$\cos(nk_0d_f) = \frac{1 - r^2 + t_0^2}{2t_0^2}, \tag{4}$$

$$Z = \sqrt{\frac{(1+r)^2 - t_0^2}{(1-r)^2 - t_0^2}}, \tag{5}$$

where $t_0 = te^{ik_0d_f}$ is called the normalized transmission coefficient and d_f is the effective thickness of the metasurface, which is exactly equal to the actual thickness a in our work [39]. Within this method, the effective refractive index n and wave impedance Z can be retrieved from the transmission coefficient t and the reflection coefficient r which are determined by FDTD simulations. Both ε_{eff} and μ_{eff} are functions of n and Z. Therefore, the final expressions for ε_{eff} and μ_{eff} are derived as $\varepsilon_{\text{eff}} = n/Z$ and $\mu_{\text{eff}} = nZ$. The Lorentzian-type dispersive spectra of ε_{eff} and μ_{eff} with different side lengths are shown in Figs. 4(a) and 4(b), respectively. There clearly exists a series of reststrahlen bands from the real part of the dispersive spectra, indicating intense Mie resonant modes. In Fig. 4(b), as $a = 1.7$ μm, when the frequency is around 1.9, 2.5, 2.7, and 3.1×10^{14} rad/s, $\varepsilon' \to \infty$ and $\mu' \to \infty$ are observed, and Mie resonances in TM and TE modes with ε/μ near-pole effects are supported, enabling heat transfer to be further enhanced [43]. Moreover, negative effective permeability and permittivity are achieved around $\omega = 1.9 \times 10^{14}$ and 2.5×10^{14} rad/s, respectively, which originate from strong magnetic and electric dipole resonances. Meanwhile, the fact that surface modes can also be induced at the interface between the effective medium and vacuum with $\mu' = -1$ or $\varepsilon' = -1$ [31] should be noted.

The near-field radiative spectral heat flux $q(\omega, T_1, T_2)$ in the TE and TM modes between two effective media are presented in Figs. 4(c) and 4(d). Note that the general calculation procedure of the near-field radiative heat flux with dispersive permeability included is elucidated in detail in Appendix C. In both the MEMT and exact solutions, we could clearly observe the heat flux enhancement effects from the Mie resonances with different orders, i.e., the magnetic dipole, the electric dipole, and higher-order ones, excited at different frequencies. Taking $a = 1.7$ μm as an example, Fig. 4(d) shows that for the MEMT-TE case, the spectral heat flux is enhanced by exciting the magnetic dipole or higher-order resonances with the μ near-pole effect, resulting in four sharp peaks at frequencies of 1.9, 2.5, 2.7, and 3.1×10^{14} rad/s. With regard to the MEMT-TM case, the peak locations are also at 1.9, 2.5, 2.7, and 3.1×10^{14} rad/s, coming from the contribution of the ε near-pole effect induced by the electric

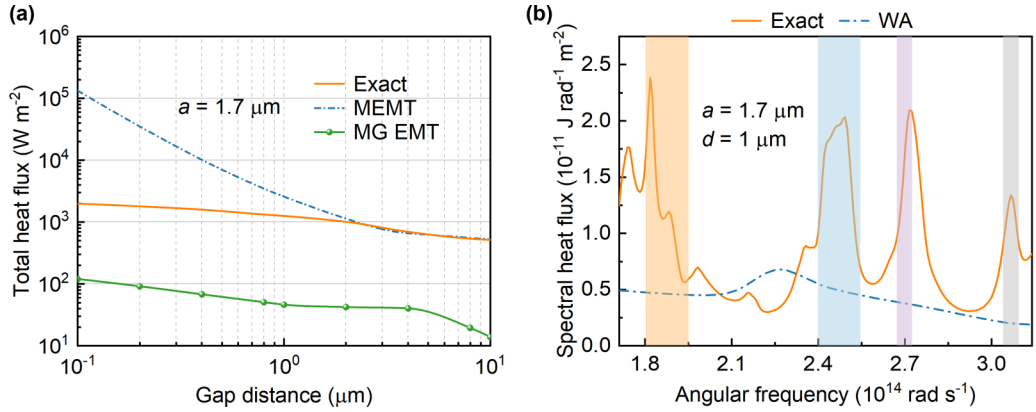

FIG. 5. (a) Total heat fluxes between two cubic dielectric resonator arrays at different vacuum gaps calculated by the exact, MEMT, and MG EMT methods. (b) Comparison of the spectral heat flux at a vacuum gap of $d = 1$ μm between the exact and WA solutions. All the emitter and receiver temperatures are set as default values.

dipole and higher-order resonance mode. Although coincident resonant peaks exist for TE and TM modes, their amplitudes are different due to different near-pole resonant intensities. It can be clearly observed that the resonant peak in TM modes is dominant due to electric resonance stronger than the magnetic counterpart at $\omega = 2.7 \times 10^{14}$ rad/s in Fig. 4(d) and 2.9×10^{14} rad/s in Fig. 4(c). Conversely, at the frequency of 3.1×10^{14} rad/s in Fig. 4(d), a more prominent spectral peak in TE modes is seen owing to a more intense magnetic response. This also demonstrates that the near-field radiative heat transfer can be spectrally enhanced for both TE and TM modes. In addition, the results of the exact and MEMT solutions clearly show the perfect consistency of the frequency for sets of heat flux peaks, providing strong evidence of the existence and enhancing effects of Mie resonances in near-field radiative heat transfer for both TE and TM modes. However, we also need to note the large discrepancy of the amplitudes for the spectral heat flux peaks between the exact and MEMT solutions. This discrepancy may be from additional magnetic and electric SP resonances, at $\mu' = -1$ and $\varepsilon' = -1$, predicted by the MEMT solution but not the exact one.

Herein, in order to further explore the reason for the discrepancy between the MEMT and exact methods, the total heat fluxes between two metasurfaces at $a = 1.7$ μm calculated by such two methods with different vacuum gaps d are shown in Fig. 5(a). It can be observed that when the vacuum gap distance is less than 2 μm, similar to the size of a cubic dielectric resonator, the total heat flux derived from the MEMT method is significantly greater than that from the exact RCWA method. However, when the vacuum gap goes beyond 2 μm, the total heat fluxes predicted by both MEMT and the exact method are almost the same. This phenomenon is consistent with the reason provided for the discrepancy between the MEMT and exact solution shown in Fig. 4(d) that the electric and magnetic SP resonances supported in the MEMT solution overestimate the heat flux compared to the exact one. With a decrease of the vacuum gap distance, the electric and magnetic SP resonances become stronger, and the discrepancy of the total heat flux between these two methods also becomes larger. On the other hand, the Maxwell-Garnett effective medium theory (MG EMT) [8], which is a commonly used EMT method in near-field radiation and regards the metasurface as a homogeneous uniaxial thin film, is examined to determine whether or not it can predict the total heat flux accurately. According to the MG EMT theory, the effective dielectric functions of the parallel and vertical components of the cubic resonator array can be expressed as

$$\varepsilon_{\parallel} = \frac{\varepsilon(1+f)+(1-f)}{\varepsilon(1-f)+(1+f)}, \tag{6}$$

$$\varepsilon_{\perp} = (1-f)+\varepsilon f, \tag{7}$$

where $f = a^2/P^2$ is the filling factor of the metasurface. For the proposed geometry, we have $f = 0.25$ ($a = 1.7$ μm). Thus, the uniaxial effective dielectric tensor of the metasurface can be given by

$$\widehat{\varepsilon} = \begin{pmatrix} \varepsilon_{\parallel} & 0 & 0 \\ 0 & \varepsilon_{\parallel} & 0 \\ 0 & 0 & \varepsilon_{\perp} \end{pmatrix}. \tag{8}$$

The total heat flux predicted by the MG EMT method is also shown in Fig. 5(a). Note that MG EMT is usually valid when the characteristic dimension of the metasurface a is much smaller than the characteristic thermal wavelength λ. And in the near-field regime, the validity of MG EMT is limited to vacuum gap distance $d > P/\pi$, as pointed out in Ref. [8]. However, we can see that the total heat flux predicted by MG EMT is far less than the exact one for any gap distance d. Contrary to previous studies [10,38], where MG EMT usually overpredicts the total heat flux due to the existence of hyperbolic modes, MG EMT would underestimate the heat transfer because it could not take into account the local resonance like Mie resonance in the present study.

In addition, a gap-based weighted approximation (WA) approach is also investigated for comparison to the exact solution with the Mie resonance excited [11]. For the two-dimensional metasurfaces that we study with $f = 0.25$, the near-field spectral heat flux $q^{\mathrm{WA}}(\omega, T_1, T_2)$ calculated by the WA method can be written as follows:

$$q^{\mathrm{WA}}(\omega, T_1, T_2) = f \times q^{\mathrm{plate}}(\omega, T_1, T_2; d), \tag{9}$$

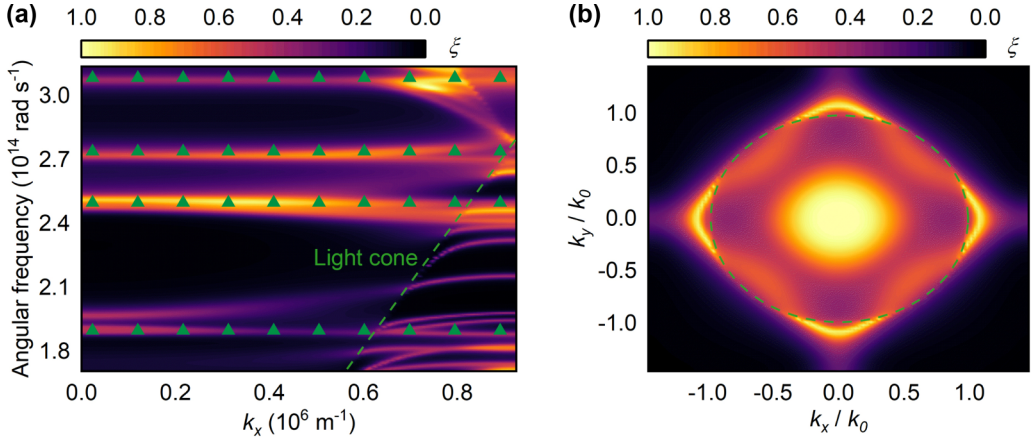

FIG. 6. (a) Contour plot of the transmission coefficient ξ from the exact solution between two Mie resonant cubic metasurfaces in the ω-k domain under $\mathbf{k}_\parallel = (k_x, 0)$ for a gap size of $d = 1$ μm and side length $a = 1.7$ μm. The Mie resonances with ε/μ near-pole effects are identified by green triangles. (b) The distribution of the transmission coefficient ξ in k_x-k_y space for the same geometry at 1.9×10^{14} rad/s. All the inserted dashed green lines denote the light cone in vacuum.

where $q^{\text{plate}}(\omega, T_1, T_2; d)$ is the spectral heat flux between two plates with a vacuum gap distance of d. By comparing the spectral heat flux from the WA method to the exact solution in Fig. 5(b), the WA method turns out to agree well with the exact result except for the regions where the Mie resonances cause spectral heat flux enhancement. This is easy to understand because the WA method could account for only the modes supported by the planar surface and not the local ones like Mie resonance excited by the cube arrays.

To get further insight into the behaviors of Mie resonance in near-field radiative transfer, we show a contour plot of the transmission coefficient ξ from exact results in the ω-k_x domain for $a = 1.7$ μm and $d = 1$ μm in Fig. 6(a). The color represents the amplitude of the transmission coefficient. Multiple bright bands, which reveal the photon tunneling channels and indicate resonant frequencies, can be clearly observed. Modes lying to the right of the light cone ($\omega = k_x c$) are a typical signature of evanescent modes, while dominant modes to the left of the light cone are propagating modes. The ε/μ near-pole modes induced by Mie resonance at frequencies of 1.9, 2.5, 2.7, and 3.1×10^{14} rad/s are indicated by triangles. Note that the enhanced transmission coefficients caused by the excitation of Mie resonances are independent of k_x. Although the Mie resonance could enhance the transmission coefficient at both propagating and evanescent waves, it could not behave like the surface modes in which the strength rapidly increases with the decrease of the vacuum gap distance. This difference could also be derived from the comparison of the total heat flux at different gap distances between the MEMT and exact solutions shown in Fig. 5(a). Furthermore, we plot the transmission coefficient ξ in k_x-k_y space at magnetic dipole resonant frequency $\omega = 1.9 \times 10^{14}$ rad/s in Fig. 6(b). The wave vector $\mathbf{k}_\parallel = (k_x, k_y)$ is normalized by the wave vector in vacuum k_0. The green dashed line denotes the light cone ($k_x^2 + k_y^2 = k_0^2$). Due to the C_4 rotational symmetry of the cubic metasurface, the transmission coefficient distribution in k_x-k_y space is also C_4 symmetric, and the magnetic dipole resonance could increase the heat transfer channels for both propagating (area inside the light cone) and evanescent (area outside the light cone) waves.

IV. CONCLUSION

In summary, we have theoretically investigated the effect of Mie resonance in the near-field radiative heat flux between two all-dielectric metasurfaces based on the exact RCWA method. It was found that the excitation of Mie resonances could cause ε/μ near-pole effects and hence enhance the spectral radiative heat flux, verified by the consistency of magnetic resonance in TE modes and electric resonance in TM modes compared to the MEMT method. Meanwhile, the applicability of MEMT in predicting near-field thermal radiation was evaluated by the exact solution, and a vacuum gap distance beyond the cubic size is needed for MEMT to be valid. The MG EMT and WA methods were also analyzed, and neither of them can predict the heat transfer correctly. The excitation of Mie resonance in near-field thermal radiation provides an innovative way to spectrally enhance heat transfer in both TM and TE modes. The fundamental understanding obtained in this paper will pave the way to tailor near-field radiative spectra with all-dielectric metamaterials for active thermal management at the nanoscale.

ACKNOWLEDGMENTS

This research was supported by the National Natural Science Foundation of China under Grant No. 51806045 and the Science, Technology and Innovation Commission of Shenzhen Municipality under Grant No. KQJSCX20170329111827540.

APPENDIX A: RIGOROUS COUPLED-WAVE ANALYSIS

Based on the exact scattering theory, near-field radiative heat flux between two metasurfaces can be given by the

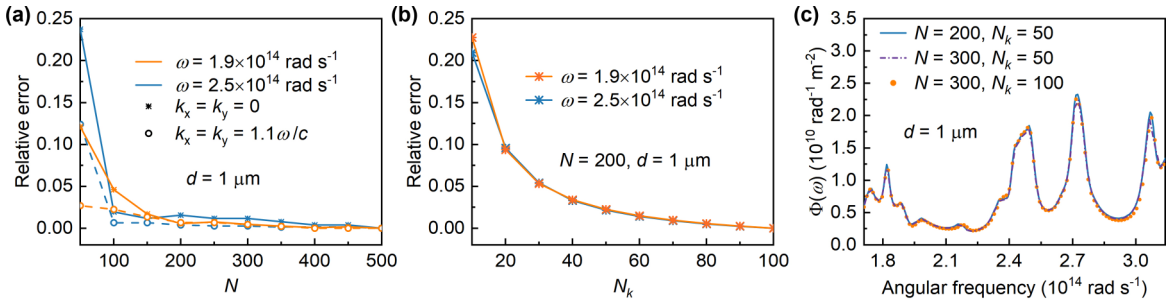

FIG. 7. Convergence test for (a) the transmission coefficient $\xi(\omega, \mathbf{k}_\parallel)$ and (b) the transmission factor $\Phi(\omega)$ between two Mie resonant cubic metasurfaces with side length $a = 1.7$ μm and vacuum gap $d = 1$ μm. The relative error varies with the maximum diffraction order N and number of k_x (k_y) points N_k, respectively. (c) The transmission factor $\Phi(\omega)$ between two metasurfaces through the RCWA method with different ranges for N and N_k.

following Landauer-like expression [44]:

$$h(T_1, T_2) = \int_0^\infty q(\omega, T_1, T_2) d\omega = \int_0^\infty [\Theta(\omega, T_1) - \Theta(\omega, T_2)]\Phi(\omega) d\omega. \quad \text{(A1)}$$

The spectral transmission factor $\Phi(\omega)$ for a two-dimensional periodic system is expressed as [7]

$$\Phi(\omega) = \frac{1}{8\pi^3} \int_{-\pi/P}^{\pi/P} \int_{-\pi/P}^{\pi/P} \xi(\omega, k_x, k_y) dk_x dk_y, \quad \text{(A2)}$$

where $\xi(\omega, \mathbf{k}_\parallel)$ is the transmission coefficient that characterizes the possibility of photon tunneling from one body to the other at a frequency ω and mode $\mathbf{k}_\parallel$. It can be decided by [10]

$$\xi(\omega, \mathbf{k}) = \mathrm{Tr}(\mathbf{D}\mathbf{W}_1\mathbf{D}^\dagger\mathbf{W}_2), \quad \text{(A3a)}$$

$$\mathbf{D} = (\mathbf{I} - \mathbf{S}_1\mathbf{S}_2)^{-1}, \quad \text{(A3b)}$$

$$\mathbf{W}_1 = \sum_{-1}^{\mathrm{pw}} -\mathbf{S}_1 \sum_{-1}^{\mathrm{pw}} \mathbf{S}_1^\dagger + \mathbf{S}_1 \sum_{-1}^{\mathrm{ew}} - \sum_{-1}^{\mathrm{ew}} \mathbf{S}_1^\dagger, \quad \text{(A3c)}$$

$$\mathbf{W}_2 = \sum_{1}^{\mathrm{pw}} -\mathbf{S}_2^\dagger \sum_{1}^{\mathrm{pw}} \mathbf{S}_2 + \mathbf{S}_2^\dagger \sum_{1}^{\mathrm{ew}} - \sum_{1}^{\mathrm{ew}} \mathbf{S}_2, \quad \text{(A3d)}$$

where $\mathbf{S}_1 = \mathbf{R}_1$, $\mathbf{S}_2 = e^{ik_{z0}d}\mathbf{R}_2 e^{ik_{z0}d}$, the dagger is the Hermitian adjoint, and $\mathbf{R}_1$ and $\mathbf{R}_2$ are the reflection matrices of the interface between the vacuum and metasurface, which can be computed by the RCWA method. The operators $\sum_{\pm 1}^{\mathrm{pw/ew}} = \frac{1}{2}k_{z0}^{\pm 1} \prod^{\mathrm{pw/ew}}$, where $\prod^{\mathrm{pw/ew}}$ are the projectors into propagating/evanescent modes and $k_{z0} = \sqrt{\omega^2/c^2 - k_\parallel^2}$ is the longitudinal wave vector in the vacuum, where $k_\parallel$ is the modulus of $\mathbf{k}_\parallel$. To get the transmission factor $\Phi(\omega)$, the transmission coefficient ξ is integrated over all of $\mathbf{k}_\parallel$. Note that $\mathbf{k}_\parallel$ is the in-plane wave vector on the interface of the vacuum and metasurface, the modulus of which can be expressed as $k_\parallel^j = \sqrt{(k_x^0 + \frac{2\pi}{p} j)^2 + (k_y^0 + \frac{2\pi}{p} j)^2}$ ($j \in \mathbb{N}$) according to the Bloch wave condition. Here $\mathbf{k}_\parallel^\mathbf{0} = (k_x^0, k_y^0)$ is the wave vector in the first Brillouin zone of the periodic lattice, j runs from $-N$ to N, and N refers to the maximum diffraction order. For more complicated geometries, the integrating value of ξ is adjusted to be rigorous by using a larger diffraction order. For the sake of saving computational costs and ensuring the numerical accuracy, the maximum diffraction order is picked on the basis of this convergence analysis.

APPENDIX B: CONVERGENCE ANALYSIS OF THE RCWA METHOD

The framework of fluctuational electrodynamics that combines scattering matrix theory with RCWA was successfully used to analyze near-field thermal radiation in Refs. [7,45]. To ensure the validation of numerical calculations using the RCWA method, we have tested the convergence of $\xi(\omega, \mathbf{k}_\parallel)$ for the proposed metasurfaces as a function of the maximum diffraction order N at a vacuum gap distance of $d = 1$ μm. For the given frequency $\omega = 1.9$ and 2.5×10^{14} rad/s, the results for $\mathbf{k}_\parallel = (0, 0)$, $(1.1\omega/c, 1.1\omega/c)$ are shown in Fig. 7(a). The relative error is defined as $e_1 = |\xi/\xi_{\mathrm{accurate}} - 1|$ to judge whether ξ is convergent, where ξ with $N = 500$ is regarded as accurate. As we can see, for the four cases considered here, as N increases from 100 to 500, the corresponding relative errors e_1 are within 5%, which indicates good convergence. The result calculated with $N = 200$ is slightly smaller than the accurate value by 1% but can save a lot of time. For the given maximum diffraction order $N = 200$ and fixed frequency, the convergence of $\Phi(\omega)$ with a change in the number of k_x (k_y) points N_k has also been checked. Here the relative error is defined as $e_2 = |\Phi/\Phi_{\mathrm{accurate}} - 1|$, in which the value of Φ at $N_k = 100$ is treated as accurate. As shown in Fig. 7(b), $N_k = 50$ was applied to calculate the spectral transmission factor with a relative error smaller than 2% compared to that obtained with $N_k = 100$. Thus, a total of 401 diffraction orders (i.e., $N = 200$) and 2500 $\mathbf{k}_\parallel$ points (i.e., $N_k = 50$) are selected in our paper. Figure 7(c) shows $\Phi(\omega)$ obtained from different parameters N and N_k. Even in the cases with $N = 300$ and $N_k = 100$, the results are also consistent, which validates the correctness of the RCWA method with the parameters applied in this work.

APPENDIX C: NEAR-FIELD RADIATIVE HEAT TRANSFER IN MAGNETIC FILMS

Near-field radiative spectral heat flux between two thin films with dispersive permittivity and permeability can be

expressed as follows [3]:

$$q(\omega, T_1, T_2) = \frac{1}{\pi^2}\int_0^\infty [\Theta(\omega, T_1) - \Theta(\omega, T_2)]d\omega \times \int_0^\infty \xi(\omega, k_\parallel)k_\parallel dk_\parallel, \tag{C1}$$

where $\xi(\omega, k_\parallel)$ is the transmission coefficient of the films,

$$\xi(\omega, k_\parallel) = \begin{cases} \frac{\left(1-\left|R_1^{p,s}\right|^2\right)\left(1-\left|R_2^{p,s}\right|^2\right)}{\left|1-R_1^{p,s}R_2^{p,s}e^{2ik_{z0}d}\right|^2}, & k_\parallel < k_0, \\ \frac{\mathrm{Im}\left(R_1^{p,s}\right)\mathrm{Im}\left(R_2^{p,s}\right)}{\left|1-R_1^{p,s}R_2^{p,s}e^{2ik_{z0}d}\right|^2}e^{2ik_{z0}d}, & k_\parallel > k_0, \end{cases} \tag{C2}$$

for propagating ($k_\parallel < k_0$) and evanescent modes ($k_\parallel > k_0$), where k_{z0} is the perpendicular component of the wave vector in vacuum and the subscripts 0, 1, and 2, respectively, denote vacuum, film emitter, and film receiver. $R_j^{p,s}$ ($j \in \{1, 2\}$) is the film refection coefficient for p or s polarization, which is defined as

$$R_j^{p,s} = \frac{r_{0j}^{p,s} + r_{j0}^{p,s}e^{2ik_{zj}a}}{1 + r_{0j}^{p,s}r_{j0}^{p,s}e^{2ik_{zj}a}}. \tag{C3}$$

In Eq. (C3), k_{zj} is the perpendicular component of the wave vector in the jth film $\mathbf{k}_j$, and $r_{j0}^{p,s}$ ($r_{0j}^{p,s}$) is the Fresnel reflection coefficient at the interface j-0 (0-j) in p or s polarization, which is given by [46]

$$r_{j0}^{p(s)} = \frac{\varepsilon_0(\mu_0)k_{zj} - \varepsilon_j(\mu_j)k_{z0}}{\varepsilon_0(\mu_0)k_{zj} + \varepsilon_j(\mu_j)k_{z0}}, \tag{C4}$$

$$r_{0j}^{p(s)} = \frac{\varepsilon_j(\mu_j)k_{z0} - \varepsilon_0(\mu_0)k_{zj}}{\varepsilon_j(\mu_j)k_{z0} + \varepsilon_0(\mu_0)k_{zj}}. \tag{C5}$$

Note that μ_0 is the permeability in vacuum, and $\varepsilon_j = \varepsilon_{\mathrm{eff}}$ ($\mu_j = \mu_{\mathrm{eff}}$) is the permittivity (permeability) of the jth film. For the transmission coefficient ξ, the contribution of the magnetic response will be included in s-polarized or TE waves, while that of the electric response belongs to p-polarized or TM waves.

[1] J. C. Cuevas and F. J. García-Vidal, ACS Photonics **5**, 3896 (2018).
[2] D. Polder and M. Van Hove, Phys. Rev. B **4**, 3303 (1971).
[3] Y. Zhang, H.-L. Yi, and H.-P. Tan, ACS Photonics **5**, 3739 (2018).
[4] S. Basu, B. J. Lee, and Z. Zhang, J. Heat Transfer **132**, 023302 (2010).
[5] S. Shen, A. Narayanaswamy, and G. Chen, Nano Lett. **9**, 2909 (2009).
[6] S. Basu, Z. Zhang, and C. Fu, Int. J. Energy Res. **33**, 1203 (2009).
[7] V. Fernández-Hurtado, F. J. García-Vidal, S. Fan, and J. C. Cuevas, Phys. Rev. Lett. **118**, 203901 (2017).
[8] S.-A. Biehs, M. Tschikin, and P. Ben-Abdallah, Phys. Rev. Lett. **109**, 104301 (2012).
[9] S.-A. Biehs and P. Ben-Abdallah, Z. Naturforsch. A **72**, 115 (2017).
[10] Y. Yang and L. Wang, Phys. Rev. Lett. **117**, 044301 (2016).
[11] Y. Yang, P. Sabbaghi, and L. Wang, Int. J. Heat Mass Transfer **108**, 851 (2017).
[12] J. Dai, S. A. Dyakov, and M. Yan, Phys. Rev. B **92**, 035419 (2015).
[13] J. Dai, S. A. Dyakov, S. I. Bozhevolnyi, and M. Yan, Phys. Rev. B **94**, 125431 (2016).
[14] C. Caloz and T. Itoh, *Electromagnetic Metamaterials: Transmission Line Theory and Microwave Applications* (Wiley, Hoboken, NJ, 2005).
[15] S. Basu and M. Francoeur, Appl. Phys. Lett. **99**, 143107 (2011).
[16] S. Basu, Y. Yang, and L. Wang, Appl. Phys. Lett. **106**, 033106 (2015).
[17] K. Joulain, J. Drevillon, and P. Ben-Abdallah, Phys. Rev. B **81**, 165119 (2010).
[18] H. Wu, Y. Huang, and K. Zhu, Opt. Lett. **40**, 4532 (2015).
[19] J. Song and Q. Cheng, Phys. Rev. B **94**, 125419 (2016).
[20] J. Song, L. Lu, Q. Cheng, and Z. Luo, J. Heat Transfer **140**, 082005 (2018).
[21] B. Guha, C. Otey, C. B. Poitras, S. Fan, and M. Lipson, Nano Lett. **12**, 4546 (2012).
[22] S. Basu and M. Francoeur, Appl. Phys. Lett. **98**, 113106 (2011).
[23] Y. Zhang, C.-L. Zhou, H.-L. Yi, and H.-P. Tan, Phys. Rev. Appl. **13**, 034021 (2020).
[24] P. Ben-Abdallah and S.-A. Biehs, Phys. Rev. Lett. **112**, 044301 (2014).
[25] Y. Yang, S. Basu, and L. Wang, J. Quant. Spectrosc. Radiat. Transfer **158**, 69 (2015).
[26] P. Sabbaghi, Y. Yang, J.-Y. Chang, and L. Wang, J. Quant. Spectrosc. Radiat. Transfer **234**, 108 (2019).
[27] S. Jahani and Z. Jacob, Nat. Nanotechnol. **11**, 23 (2016).
[28] Q. Zhao, J. Zhou, F. Zhang, and D. Lippens, Mater. Today **12**, 60 (2009).
[29] F. J. Bezares, J. P. Long, O. J. Glembocki, J. Guo, R. W. Rendell, R. Kasica, L. Shirey, J. C. Owrutsky, and J. D. Caldwell, Opt. Express **21**, 27587 (2013).
[30] K. Takano, Y. Yakiyama, K. Shibuya, K. Izumi, H. Miyazaki, Y. Jimba, F. Miyamaru, H. Kitahara, and M. Hangyo, IEEE Trans. Terahertz Sci. Technol. **3**, 812 (2013).
[31] M. Francoeur, S. Basu, and S. J. Petersen, Opt. Express **19**, 18774 (2011).
[32] Y. Bai, Y. Jiang, and L. Liu, J. Quant. Spectrosc. Radiat. Transfer **158**, 36 (2015).
[33] L. Lu, J. Song, K. Zhou, and Q. Cheng, in *ASME 2019 6th International Conference on Micro/Nanoscale Heat and Mass Transfer*, American Society of Mechanical Engineers Digital Collection (American Society of Mechanical Engineers, Dalian, China, 2019).
[34] Z. Zheng and Y. Xuan, Chin. Sci. Bull. **56**, 2312 (2011).
[35] S. J. Petersen, S. Basu, and M. Francoeur, Photonics Nanostruct. Fundam. Appl. **11**, 167 (2013).

[36] A. Ghanekar, Y. Tian, S. Zhang, Y. Cui, and Y. Zheng, Materials **10**, 885 (2017).
[37] S. J. Petersen, S. Basu, B. Raeymaekers, and M. Francoeur, J. Quant. Spectrosc. Radiat. Transfer **129**, 277 (2013).
[38] X. Liu and Z. Zhang, ACS Photonics **2**, 1320 (2015).
[39] J. C. Ginn, I. Brener, D. W. Peters, J. R. Wendt, J. O. Stevens, P. F. Hines, L. I. Basilio, L. K. Warne, J. F. Ihlefeld, P. G. Clem *et al.*, Phys. Rev. Lett. **108**, 097402 (2012).
[40] K. Chen, B. Zhao, and S. Fan, Comput. Phys. Commun. **231**, 163 (2018).
[41] T. Liu, R. Xu, P. Yu, Z. Wang, and J. Takahara, Nanophotonics **9**, 1115 (2020).
[42] D. R. Smith, S. Schultz, P. Markoš, and C. M. Soukoulis, Phys. Rev. B **65**, 195104 (2002).
[43] J.-Y. Chang, P. Sabbaghi, and L. Wang, Int. J. Heat Mass Transfer **158**, 120023 (2020).
[44] S.-A. Biehs, F. S. Rosa, and P. Ben-Abdallah, Appl. Phys. Lett. **98**, 243102 (2011).
[45] R. Messina, A. Noto, B. Guizal, and M. Antezza, Phys. Rev. B **95**, 125404 (2017).
[46] S. Basu and M. Francoeur, Opt. Lett. **39**, 1266 (2014).